Electrostatic Self-Assembly of Polydiacetylene Nanocrystals: Nonlinear Optical Properties and Chain Orientation

Jin-An He, Ke Yang, Jayant Kumar, and Sukant K. Tripathy*

Center for Advanced Materials, Departments of Chemistry and Physics, University of Massachusetts Lowell, Lowell, Massachusetts 01854

Lynne A. Samuelson

Materials Science Team, U.S. Army Soldier & Biological Chemical Command, Soldier Systems Center, Natick, Massachusetts 01760

Toshiyuki Oshikiri, Hideyuki Katagi, Hitoshi Kasai, Shuji Okada, Hidetoshi Oikawa, and Hachiro Nakanashi

Institute for Chemical Reaction Science, Tohoku University, Sendai 980-77, Japan

Received: July 28, 1999; In Final Form: October 19, 1999

Two different sizes of nanocrystals of poly(1,6-dicarbazolyl-2,4-hexadiyne) (poly-DCHD), have been assembled into composite films by electrostatic self-assembly (ESA) using poly(dimethyldiallylammonium chloride) (PDAC) as the oppositely charged polyelectrolyte. UV−visible absorption showed that the film deposition process is uniform. The AFM images of these films indicate that the nanocrystals are platelets lying on the substrate plane. The chromophore (polydiacetylene backbone) orientation and third-order optical nonlinearity of poly-DCHD/PDAC multilayers are investigated by electroabsorption spectroscopy. The ratio of $\chi^{(3)}_{3333}$ to $\chi^{(3)}_{1133}$ is significantly less than 3, indicating that the polymer chains are predominantly parallel to the plane of the substrate. In addition, the films possess third-order nonlinearity in the order of 10^{-11} esu.

1. Introduction

Nanosized materials, based on their unique optical, electronic, and chemical features due to their specific sizes and composition, have attracted much attention over the past decade.[1−3] Numerous types of metal and semiconductor nanoparticles have been produced by various chemical and physical methods, and the applications of these inorganic nanometer-scale materials have impacted on a number of different areas such as catalysis, sensor technologies, optics, and electronics among others.[4−6] However, the synthesis and property studies, especially electronic and photonic properties, on organic and especially polymeric nanostructured materials are rather limited.[7]

Polydiacetylenes (PDA) are a unique class of single crystalline polymers that are produced by topochemical polymerization in the solid state in single crystals of the diacetylene monomer.[8] Due to the unusual structural as well as electronic and optical properties of PDA, this unique class of polymers has been extensively investigated.[9,10] Large anisotropy of electrical conductivity has been observed in single crystals and oriented PDA films.[11,12] The polymers possess large third-order optical nonlinearities due to the substantial π-electron delocalization along the main chain backbones, i.e., the one-dimensional conjugated structure.[13,14] The nonresonant third-order nonlinear optical (NLO) susceptibility in the chain direction of the anisotropic crystals is one of the largest recorded to date.[15] Recently, Nakanishi and co-workers have developed a facile process to prepare nanocrystals of PDAs in a water suspension.[16,17] Disk-like nanoparticles of poly-DCHD have been produced using solid-state topochemical polymerization within the monomer microcrystals in the aqueous medium. These polymeric nanoparticles possess unique electronic and optical properties due to their size effect, as had been observed in several types of inorganic nanocrystals.[18]

Utilization of the unique properties of these polymeric nanoparticles requires them to be processed into ordered assemblies with good optical quality. Several fabrication methods of thin single crystals of PDAs as well as spin-coated and Langmuir−Blodgett (LB) thin films of PDAs have been carried out.[19−22] To form uniform large area, a thin single crystal of PDAs is nontrivial.[19] On the other hand, the NLO properties of PDA thin films obtained by spin-coating or LB technique are compromised compared to those of single crystals due to the distortion of the π-conjugated main backbones of PDAs.[21,22] Recently, Tripathy and co-workers used polycation as the oppositely charged matrix to adsorb poly-DCHD nanocrystals, and multilayers of polycation/poly-DCHD nanocomposite assemblies were effectively fabricated by the electrostatic layer-by-layer self-assembly (ESA) technique.[23] In this work, uniform multilayers containing poly-DCHD nanocrystals were obtained and verified by UV−visible absorption spectroscopy and scanning electron microscopy.

The ESA technique, which produces thin multilayers on solid supports by the spontaneous adsorption of oppositely charged polyelectrolytes from their dilute aqueous solution, is a facile method in that it allows the structure, composition, and thickness of the film to be adjusted and controlled.[24] Furthermore, the method has been developed and applied to other charged species, such as inorganic nanoparticles, dyes, proteins and enzymes, nucleic acids, and functional polymers.[25] We have utilized this

* Corresponding author.

10.1021/jp992633+ CCC: $18.00
Published on Web 11/24/1999

technique to fabricate second-order NLO azo polymer films by successfully aligning the azo chromophores into a noncentrosymmetric arrangement.[26] These films produced second-order NLO response comparable to and in some cases even better than the corresponding spin-coated and poled films. The polymer films were isotropic in the plane of the film; however, acentric alignment of the chromophores was achieved normal to the film plane. Acentric assembly of the purple membrane fragments was also achieved for the first time utilizing this approach.[27]

In this paper we have extended the ESA technique to prepare multilayer films of the PDAC/poly-DCHD nanocrystals. The third-order NLO response of the composite multilayers has been investigated. The tensorial components of the measured third-order nonlinearity have been further used to establish the nature of the chain orientation and hence the anisotropic crystalline alignment. Based on our earlier studies,[23] the detailed solution conditions for preparation of polycation/poly-DCHD nanoparticle (two different sizes) multilayers are first presented. Comparative characterizations of the films containing different sized poly-DCHD particles, including absorption spectra and atomic force microscopy (AFM), confirm that uniform polycation/poly-DCHD nanocrystal multilayers have been obtained. Electroabsorption spectroscopes of the films are performed in order to obtain the tensorial components of the third-order NLO susceptibilities of these films. These films show appreciable third-order NLO susceptibilities in the order of 10^{-11} esu. Further, the π-conjugated main chain backbone of poly-DCHD nanoparticles is found to be predominantly parallel to the plane of the substrate, thus indicating preferential adsorption of the crystal planes containing the polymer chain backbones.

2. Materials and Methods

2.1. Materials. Poly-DCHD nanocrystals were prepared using 1,6-dicarbazolyl-2,4-hexadiyne (DCHD) monomer dispersions in water and subsequent solid-state photopolymerization by 254-nm UV irradiation.[28,29] The detailed procedure for the preparation of poly-DCHD microcrystals can be found in our previous work.[16,17,28,29] Briefly, 100 to 200 μL of DCHD acetone solution (concentration $\sim 10^{-2}$ M) was rapidly injected into 10 mL of distilled water. The resultant dispersion was stirred vigorously for 20 min. As acetone from monomer solution droplets diffuses away into the water bath, nanoparticles of the monomer are formed and suspended in water. Crystallization in the monomer nanoclusters follows, and UV irradiation using the 254-nm line from a high-pressure mercury lamp was carried out for 20 min to prepare poly-DCHD nanoparticles as a result of solid-state photopolymerization. The shape and size of the formed poly-DCHD microcrystals are dependent on the dispersion time and concentration of DCHD monomer in the reaction system.[29] In the present work, we prepared two differently sized poly-DCHD samples which are 100 nm for the larger sized (named as large poly-DCHD nanoparticles) and 50 nm for smaller sized poly-DCHD nanocrystals (named as small poly-DCHD nanoparticles) measured by scanning electron microscopy, respectively.[23,29] Poly(dimethyl diallylammonium chloride) (PDAC, 20 wt % in water, M_w 200,000−350,000) was purchased from Aldrich and was used as received. The molecular structures used in the multilayer deposition are shown in Figure 1.

2.2. Layer-by-Layer Deposition. Polycationic PDAC was dissolved in Milli-Q water at a concentration of 2.0 mg/mL (12.4 mM based on the repeat unit molecular weight), containing 0.5 M NaCl and at a pH of 6.8 for the multilayer adsorption. The fabrication procedure of the poly-DCHD/PDAC multilayers is described as follows. A negatively charged glass slide (KOH solution partially hydrolyzes the surface) is primed by adsorbing a layer of PDAC on its surface (2 mg/mL PDAC, 5 min). After being rinsed with water the primed substrate is immersed into the poly-DCHD aqueous suspensions (3.2×10^{-2} mg/mL, 0.08 mM based on the repeat unit molecular weight) for 5 min, then rinsed with water for 2 min. This process is repeated until the desired number of bilayers of poly-DCHD/PDAC multilayer is obtained.

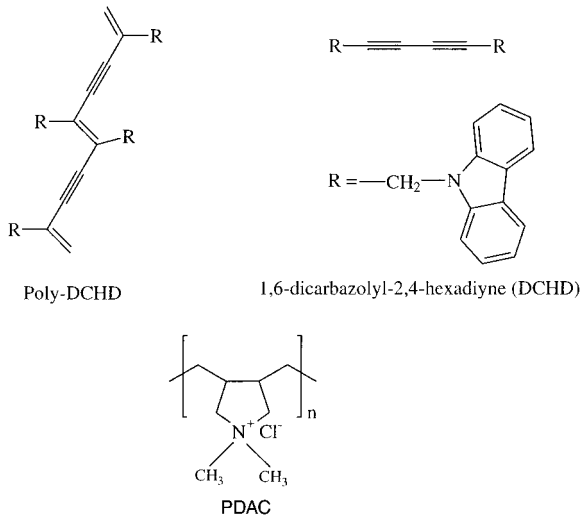

Figure 1. Structures of the polydiacetylene and polyelectrolyte for the ESA assembly.

2.3. Sample Characterization. UV−visible absorption spectra were obtained for the solutions of the poly-DCHD nanocrystals and for the deposited films using a Perkin-Elmer Lambda-9 UV−vis/near-infrared spectrophotometer. Thickness measurements were carried out with a Rudolph Research type 43603-200E ellipsometer. AFM observations were performed with an atomic force microscope (Park Scientific, CA) operated in the noncontact mode using a standard silicon nitride cantilever (force constant 0.03 N/m). The setpoint is -0.12 μm. The films were deposited onto silicon wafers and scanned at the rate of 1 l/s (one line per second) in ambient air.

2.4. Electroabsorption Spectroscopy. Electroabsorption spectroscopy was performed to determine the dispersions of the third order NLO susceptibilities and to obtain orientation information about the chromophores. The technique relies on the sensitive detection of the Stark shift with the application of the external electric field which leads to the absorbance changes of the sample. The detailed theoretical background about this spectroscopic technique is presented in our earlier papers and is further briefly described in the theory section.[30−33] The experimental setup is shown in Figure 2. ITO-coated glass slides were used to prepare PDAC/poly-DCHD multilayers. Thirty bilayers of large and small-sized poly-DCHD/PDAC multilayers were deposited onto the ITO electrodes: the thickness of the films is measured to be about 56 nm for the large-sized poly-DCHD and 134 nm for the small-sized poly-DCHD nanocrystals by ellipsometric thickness measurements. On top of the polymer films, a layer of aluminum film ($\sim$30 nm) was thermally evaporated onto the assembly as the counter electrode. A sinusoidal electric field ($E_{ac} = E_{ac0}\cos\Omega t$, $\Omega = 2\pi f$, $f = 1$ kHz, $V_{p-p} = 25.5$ V) was applied to the sample. *p*-Polarized light from a 50 W tungsten lamp through a monochromator was irradiated on the sample at oblique incidence angles. The electroabsorption signal $\Delta I_{2\Omega}$, which is defined as the change in the output intensity I at twice the modulation frequency, was detected by a lock-in amplifier in $2f$ mode. The output intensity

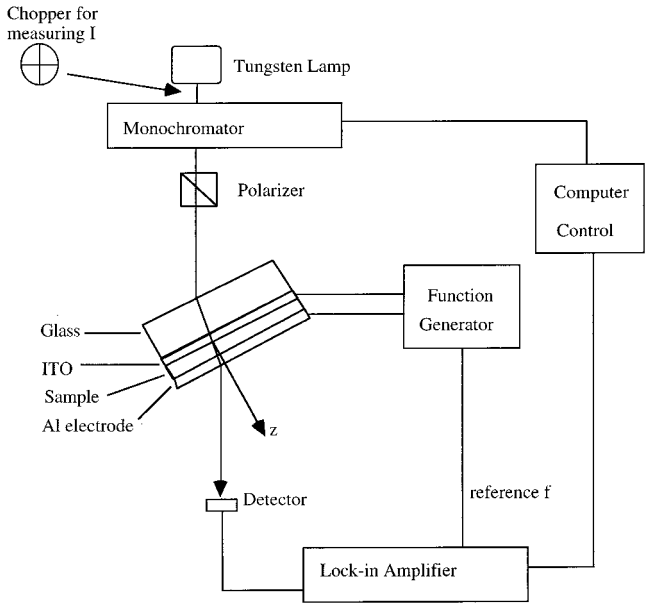

Figure 2. Setup for electroabsorption spectroscopy.

I was measured by using a chopper and without the electric field applied to the sample. The sign of $\Delta I_{2\Omega}$ was determined by comparing the amplified signal from the lock-in amplifier and the reference signal from the function generator simultaneously on an oscilloscope. A microcomputer was used to synchronize the change of wavelength selected by the monochromator and the data collection by the lock-in amplifier.

The electroabsorption spectra of PDAC/poly-DCHD self-assembled films were recorded from 450 to 750 nm at the normal and oblique incident angles. The dispersions of the real and imaginary parts of the complex refractive index, $\tilde{n} = n + i\kappa$, of the multilayers were measured using an ellipsometer (Rudolph Research, type 43603-200E) and a spectrometer (Perkin-Elmer Lambda-9). The results of $\Delta I_{2\Omega}/I$ and the complex refractive index $\tilde{n}$ were used to calculate the third-order NLO susceptibilities $\chi^{(3)}_{1133}$ and $\chi^{(3)}_{3333}$ based on the relationships presented in the theory section.

3. Theory

Let us consider the case of tilted incidence of electroabsorption spectroscopy with *p*-polarization (see Figure 2 for the experimental setup). The expression for $\Delta I_{2\Omega}/I$ is given in ref 30 as

$$\frac{\Delta I_{2\Omega}}{I} = -2\pi \frac{\omega}{c} t_k E_{aco}^2 \, 3\mathrm{Im}\left(\frac{\chi^{(3)}_{eff}}{\tilde{n}\cos\theta}\right) \tag{1}$$

where ñ is the complex refractive index of the absorptive sample, θ is the complex angle of light propagation inside the material, which is related to the angle of incidence θ_o by Snell's law: $n_o \sin\theta_o = \tilde{n} \sin\theta$ ($n_o = 1$), t_k is the sample thickness, and E_{aco} is the amplitude of the applied electric field. $\chi^{(3)}_{eff}$ is given by

$$\chi^{(3)}_{eff} = \chi^{(3)}_{1133} \cos^2\theta + \chi^{(3)}_{3333} \sin^2\theta \tag{2}$$

By measuring $\Delta I_{2\Omega}/I$, we can determine the imaginary part of the complex quantity

$$\chi^{(3)\prime}_{eff} = \frac{\chi^{(3)}_{eff}}{\tilde{n}\cos\theta} = \frac{\chi^{(3)}_{1133}\cos^2\theta + \chi^{(3)}_{3333}\sin^2\theta}{\tilde{n}\cos\theta} \tag{3}$$

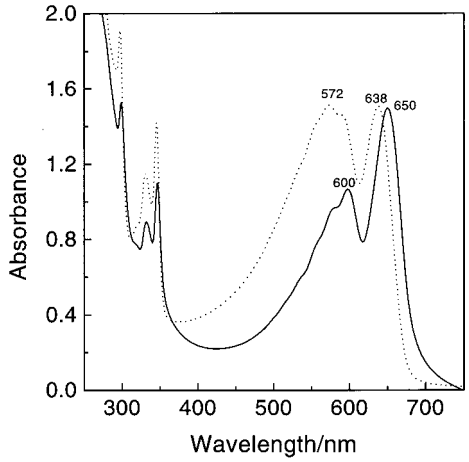

Figure 3. UV−visible absorption spectra of the aqueous suspensions, pH 9.5 of the large poly-DCHD nanocrystal (solid curve) and the small poly-DCHD nanocrystal (dot curve).

Its real part can be obtained from the Kramers−Kronig relation

$$\mathrm{Re}[\chi^{(3)\prime}_{eff}(\omega)] = \frac{2}{\pi}\int_{\omega_i}^{\omega_f} \frac{\omega' \, d\omega'}{\omega'^2 - \omega^2} \mathrm{Im}[\chi^{(3)\prime}_{eff}(\omega')] \tag{4}$$

where ω_i and ω_f are initial and final optical frequencies, respectively. The complex variable $\chi^{(3)\prime}_{eff}$ is thus obtained.

For normal incidence, $\theta = \theta_o = 0$, which leads to $\chi^{(3)\prime}_{eff}$ $(\theta = 0) = 1/\tilde{n}\ \chi^{(3)}_{1133}$, and $\chi^{(3)}_{1133}$ are determined. At tilted incidence, $\chi^{(3)}_{3333}$ is determined from the expression of $\chi^{(3)\prime}_{eff}$, which gives

$$\chi^{(3)}_{3333} = \left(\frac{\tilde{n}}{\cos\theta}\chi^{(3)\prime}_{eff}\bigg|_{\text{tilted}} - \chi^{(3)}_{1133}\right)\left(\frac{\tilde{n}^2}{\sin^2\theta_0}\bigg|_{\text{tilted}} - 1\right) \tag{5}$$

By measuring $\tilde{n} = n + i\kappa$ and determining $\chi^{(3)\prime}_{eff}$ through electroabsorption spectroscopy and the Kramers−Kronig relation, $\chi^{(3)}_{1133}$ and $\chi^{(3)}_{3333}$ could be determined independently without assuming the relation $\chi^{(3)}_{3333} = 3\chi^{(3)}_{1133}$, which is appropriate only for isotropic distribution of chromophores.[34]

4. Results and Discussion

4.1. Absorption Spectra of Poly-DCHD Aqueous Solution. Figure 3 shows the UV−vis absorption spectra of aqueous suspensions (pH 9.5, 0.08 mM based on the polymer repeat unit) of two different sizes of poly-DCHD nanocrystals. The spectral features are in accordance with those reported earlier.[23,29] From the figure, we note certain differences between the two types of nanoparticles. The absorption peaks of large poly-DCHD nanoparticles (solid curve) are shifted to longer wavelengths relative to those of small poly-DCHD nanoparticles (dotted curve). The red shifts indicate that the effective electron delocalization lengths of the main backbone chromophore (polydiacetylene chain) in the large and small poly-DCHD nanocrystals are different. The larger electron delocalization length of the main backbone shifts the absorption peak to a longer wavelength. The spectral results are consistent with the size distribution of poly-DCHD nanoparticles. These results have been further elaborated upon elsewhere.[16−18,28]

4.2. Characterization of PDAC/Poly-DCHD Nanocomposite Films. The driving force in the ESA technique for multilayer growth is primarily the electrostatic attraction and complex formation between the oppositely charged species deposited.[24] Alternating the deposition routine for charged and neutral polymers by hydrogen bonding interaction has also been demonstrated recently.[35] The surface charge features of poly-

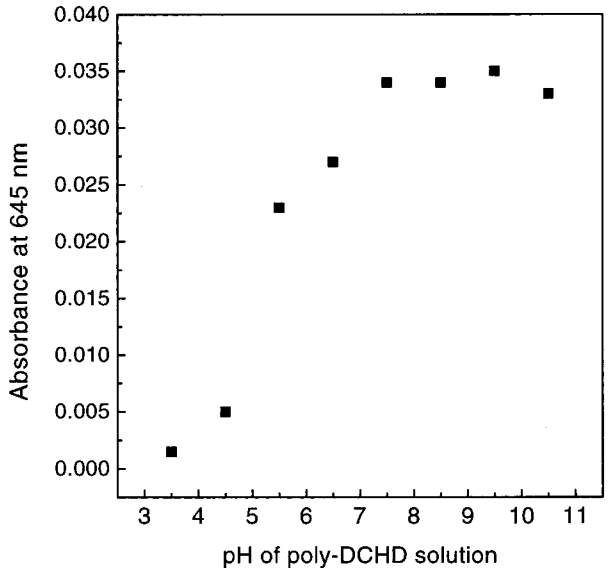

Figure 4. The relative adsorbed amount of large poly-DCHD nanocrystals characterized by its absorption at 645 nm in the (large poly-DCHD/PDAC)$_2$ assembly as a function of pH of large poly-DCHD dipping suspensions.

SCHEME 1. Proposed Electric Double Layer of Poly-DCHD Nanocrystal in Water

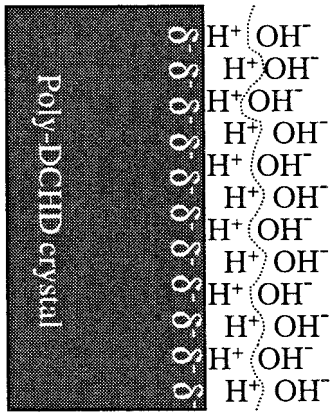

DCHD nanocrystals have been studied by measurement of its zeta (ξ) potential.[29] The value of the ξ potential of poly-DCHD nanocrystals in pure water was negative, which indicated a net negative charge on the surface of the nanocrystals. The origin of the charge distribution on poly-DCHD nanoparticles is proposed to come from the electric double layer on the surface of poly-DCHD microcrystals.[29] The presence of a π-electron rich polydiacetylene backbone, as well as the carbazolyl side groups, implies strong nucleophilicity for the poly-DCHD macromolecule. The postulated electric double layer structure at the poly-DCHD nanoparticle/water interface is shown in Scheme 1. The protons (H^+) from dissociated H_2O are first adsorbed on the surface of poly-DCHD due to its strong nucleophilicity. The next adsorbed outerlayer is formed by the hydroxyl ions (OH^-) which makes the poly-DCHD nanocrystal surface negatively charged. This proposed model implies that the surface charge density of poly-DCHD nanoparticles should increase with the concentration increase of hydroxyl groups in the solution. Our electrostatic assembly experiments, using poly-DCHD suspensions with various pH values as the polyanionic dipping solutions and PDAC as the polycationic solution, confirm this assumption. Utilizing the absorption of poly-DCHD nanocrystal at 645 nm to monitor the adsorbed amount of poly-DCHD on the PDAC layer, the dependence of the absorbance

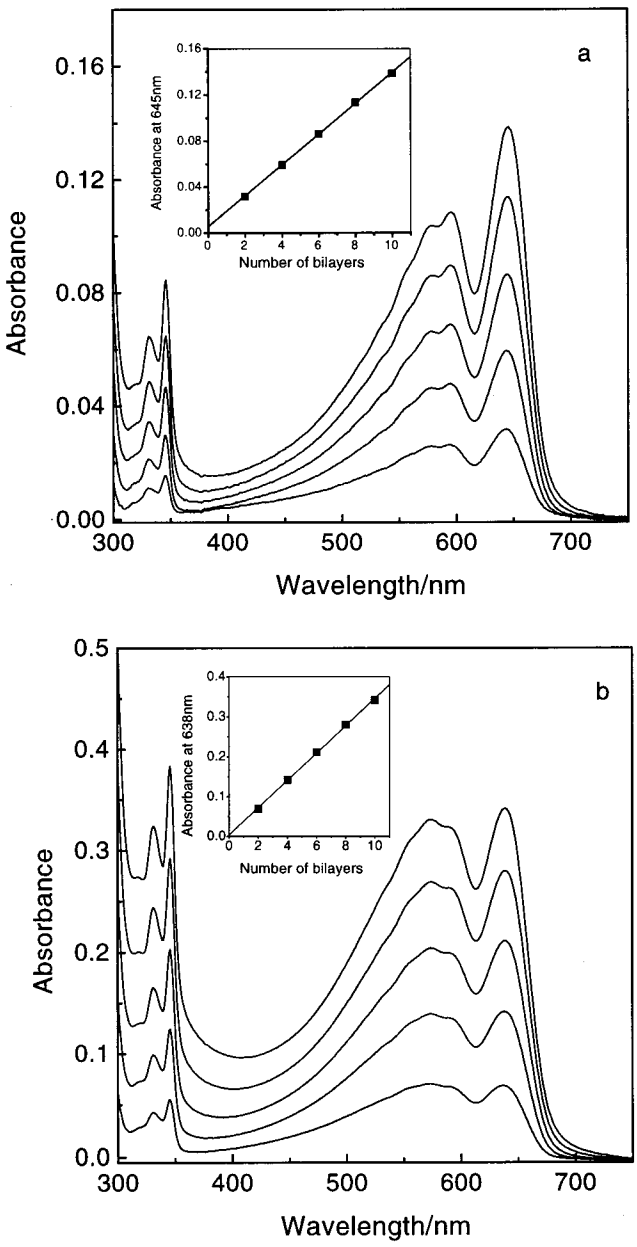

Figure 5. UV−visible consecutive absorption spectra of poly-DCHD/PDAC nanocomposite multilayers on a quartz slide: (a) for large and (b) for small poly-DCHD nanoparticles. The curves correspond to adsorption of 2, 4, 6, 8, and 10 poly-DCHD/PDAC bilayers, respectively. The insets show the linear increases of absorbance with the number of bilayers.

of (large poly-DCHD/PDAC)$_2$ films at 645 nm on the pH of the large poly-DCHD aqueous suspensions was measured and the results are presented in Figure 4. From the figure we can clearly see that the absorbance at 645 nm, in other words the relative adsorbed amount of large poly-DCHD nanocrystals, increased with the increase in pH from 3.5 to 10 of poly-DCHD suspensions. The relative adsorbed amount of the small poly-DCHD nanoparticles on the PDAC layer as a function of pH of small poly-DCHD solutions shows very similar behavior compared with that of the larger poly-DCHD nanocrystals. Based on the above results, the ESA growth of PDAC/poly-DCHD multilayers was carried out in the present system by controlling the pH of the poly-DCHD solution at 9.5.

Figure 5 shows the UV−vis absorption spectra for the multilayers prepared by sequential deposition of PDAC/poly-DCHD bilayers (Figure 5a for large poly-DCHD nanoparticles

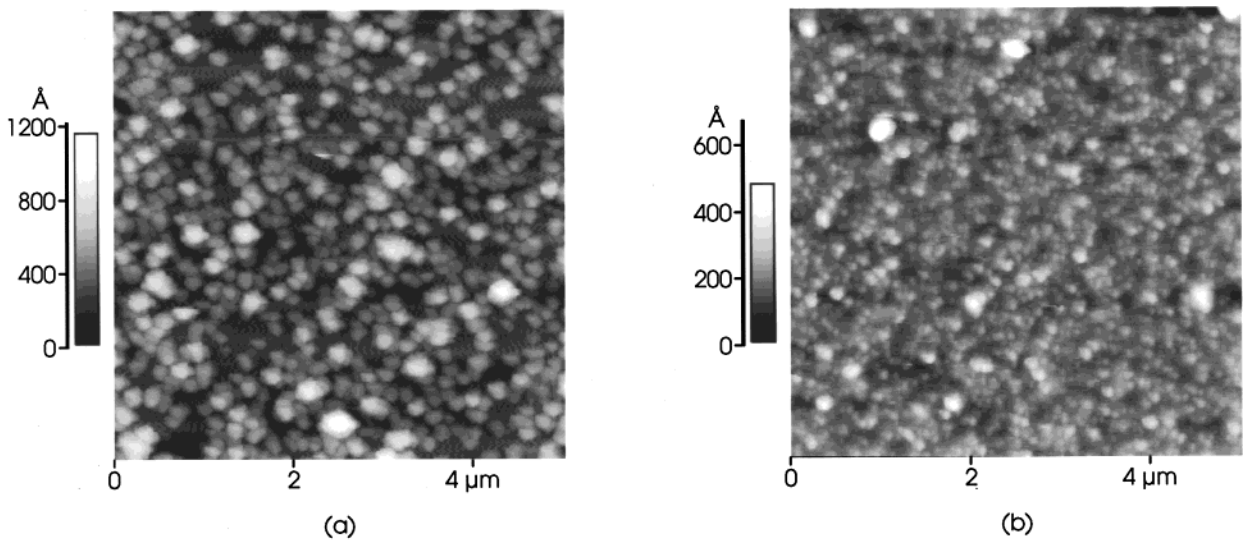

Figure 6. AFM images of (a) one bilayer of the large poly-DCHD/PDAC and (b) one bilayer of the small poly-DCHD/PDAC with poly-DCHD nanocrystals as the outer layer.

TABLE 1: Third-Order NLO Coefficients of the Large Poly-DCHD/PDAC Film

wavelength/ nm	$\mathrm{Im}[\chi^{(3)}_{3333}]$ $\times 10^{11}$ esu	$\mathrm{Im}[\chi^{(3)}_{1133}]$ $\times 10^{11}$ esu	$\mathrm{Im}[\chi^{(3)}_{3333}]/\mathrm{Im}[\chi^{(3)}_{1133}]$	wavelength/ nm	$\mathrm{Re}[\chi^{(3)}_{3333}]$ $\times 10^{11}$ esu	$\mathrm{Re}[\chi^{(3)}_{1133}]$ $\times 10^{11}$ esu	$\mathrm{Re}[\chi^{(3)}_{3333}]/\mathrm{Re}[\chi^{(3)}_{1133}]$
595	−0.33	−0.30	1.10	605	−0.35	−0.28	1.25
614	0.46	0.44	1.05	627	0.79	0.74	1.07
646	−2.01	−1.52	1.32	659	−2.44	−1.79	1.36
671	1.74	1.30	1.34	685	0.50	0.31	1.61

and Figure 5b for small nanoparticles) at each consecutive step of the multilayer growth process. As shown, the multilayer adsorption of the PDAC/poly-DCHD assemblies is linear and reproducible with deposition cycles. The absorbance at 645 nm for large poly-DCHD nanoparticles and that at 638 nm for small poly-DCHD nanoparticles are observed to increase linearly with the number of bilayers, as shown in the inset of Figure 5. These results confirm the regular stepwise growth of the films.

Figure 6 shows AFM images of one bilayer of PDAC/large poly-DCHD nanoparticles (Figure 6a) and one bilayer of PDAC/small poly-DCHD particles (Figure 6b) with poly-DCHD as the outer layer. Atomic force microscopy images of deposited PDAC/poly-DCHD nanocomposite bilayers indicate that the films are uniform. In the AFM images, regular thin platelet nanoclusters (about 160 nm across for large poly-DCHD and 100 nm across for small poly-DCHD) can be observed and are uniformly packed on the surface. From the images of the scanning electron micrographs (SEM) for the poly-DCHD particles, the size of the larger poly-DCHD particles is determined to be 100 nm and smaller particles are 50 nm.[23] The discrepancy in size determined by AFM and SEM may be due to tip convolution effects which are usually observed when using an AFM image to analyze the dimension of objects.[36] AFM morphological observations presented here further show that the strong electrostatic interaction between the negatively charged poly-DCHD surface and the polycationic PDAC results in the appearance of a highly uniform nanocomposite film by the ESA deposition.

4.3. Orientation and Third-Order Nonlinearity Studies. Electroabsorption spectroscopy can be used to characterize third-order NLO susceptibilities and the NLO chromophore orientation for interesting materials.[30−33,37,38] We have used electroabsorption with normal and oblique incidence of *p*-polarized light to determine the complex dispersions of $\chi^{(3)}_{1133}$ and $\chi^{(3)}_{3333}$. The hypothetical relationship $\chi^{(3)}_{3333} = 3\chi^{(3)}_{1133}$ for isotropic distribution of the chromophore is not used in our method;[34] instead, the ratio of $\chi^{(3)}_{3333}$ to $\chi^{(3)}_{1133}$ can be explicitly calculated from the complex spectra of $\chi^{(3)}_{1133}$ and $\chi^{(3)}_{3333}$. If the ratio of $\chi^{(3)}_{3333}$ to $\chi^{(3)}_{1133}$ is more than 3, it indicates that the NLO chromophores are inclined perpendicular to the film plane. The chromophores are isotropically oriented in three dimensions if the ratio is equal to 3. If the ratio is less than 3, the chromophores are preferentially oriented in the film plane.[30−33]

The dispersions of $\chi^{(3)}_{1133}$ and $\chi^{(3)}_{3333}$ for 30 bilayers of PDAC/larger sized poly-DCHD nanoparticle multilayers are shown in Figure 7a and 7b, respectively. From these figures we can see that their shapes are very similar between $\mathrm{Re}[\chi^{(3)}_{3333}]$ and $\mathrm{Re}[\chi^{(3)}_{1133}]$ or $\mathrm{Im}[\chi^{(3)}_{3333}]$ and $\mathrm{Im}[\chi^{(3)}_{1133}]$. The average ratios of $\mathrm{Re}[\chi^{(3)}_{3333}]$ to $\mathrm{Re}[\chi^{(3)}_{1133}]$ and $\mathrm{Im}[\chi^{(3)}_{3333}]$ to $\mathrm{Im}[\chi^{(3)}_{1133}]$, which characterize the chromophore orientation relative to the substrate, are somewhat different at different wavelengths, yet they are very close to the average ratio of 1.3 (see Table 1). This ratio is far less than 3, which indicates that the orientation of the conjugating main backbone of the larger sized poly-DCHD is predominantly along the plane of the solid support.

The electroabsorption spectra of poly-DCHD nanoparticles are consistent with their absorption spectra. In fact, the spectra of $\mathrm{Im}[\chi^{(3)}_{1133}]$ and $\mathrm{Im}[\chi^{(3)}_{3333}]$ can be explained as coming from the red shift of the absorption spectrum due to the applied external electric field, which results in the generation of a positive peak at longer wavelength and a negative peak at shorter wavelength in the electroabsorption spectrum from a single absorption peak.[30] For the large poly-DCHD nanocrystals, the main backbone produces two absorption peaks at 600 and 650 nm and a shoulder near 580 nm (see Figure 3). The positive and negative electroabsorption bands generated from the absorption peak of 600 nm are located near 614 and 595 nm, respectively, in $\mathrm{Im}[\chi^{(3)}_{1133}]$ and $\mathrm{Im}[\chi^{(3)}_{3333}]$, shown in Figure 7a and 7b. Similarly, the positive band and negative band generated from

TABLE 2: Third-Order NLO Coefficients of the Small Poly-DCHD/PDAC Film

wavelength/ nm	Im[$\chi^{(3)}_{3333}$] $\times 10^{11}$ esu	Im[$\chi^{(3)}_{1133}$] $\times 10^{11}$ esu	Im[$\chi^{(3)}_{3333}$]/ Im[$\chi^{(3)}_{1133}$]	wavelength/ nm	Re[$\chi^{(3)}_{3333}$] $\times 10^{11}$ esu	Re[$\chi^{(3)}_{1133}$] $\times 10^{11}$ esu	Re[$\chi^{(3)}_{3333}$]/ Re[$\chi^{(3)}_{1133}$]
592	−0.29	−0.48	0.60	600	−0.32	−0.39	0.82
608	0.19	0.35	0.54	618	0.37	0.86	0.43
635	−0.92	−1.92	0.48	650	−1.61	−2.74	0.59
663	1.28	2.10	0.61	680	0.41	0.76	0.54

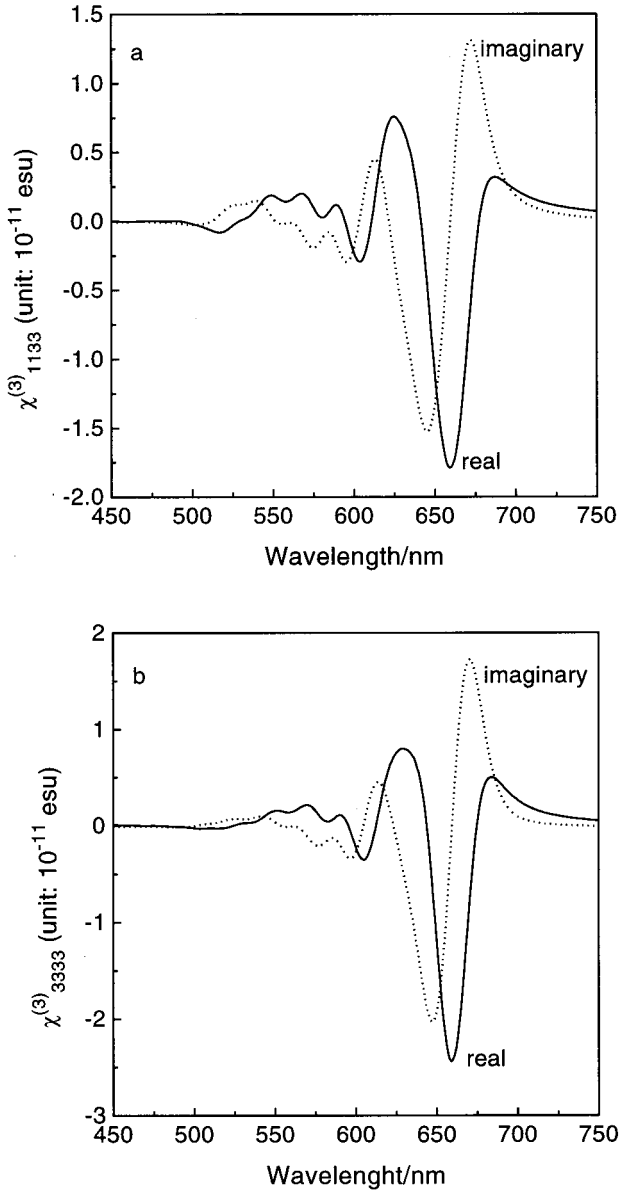

Figure 7. (a) Dispersion of $\chi^{(3)}_{1133}$ of 30 bilayers of the large poly-DCHD/PDAC film. Uncertainty: $\pm 9.0 \times 10^{-13}$ esu. (b) Dispersion of $\chi^{(3)}_{3333}$ of 30 bilayers of the large poly-DCHD/PDAC film. Uncertainty: $\pm 1.8 \times 10^{-12}$ esu.

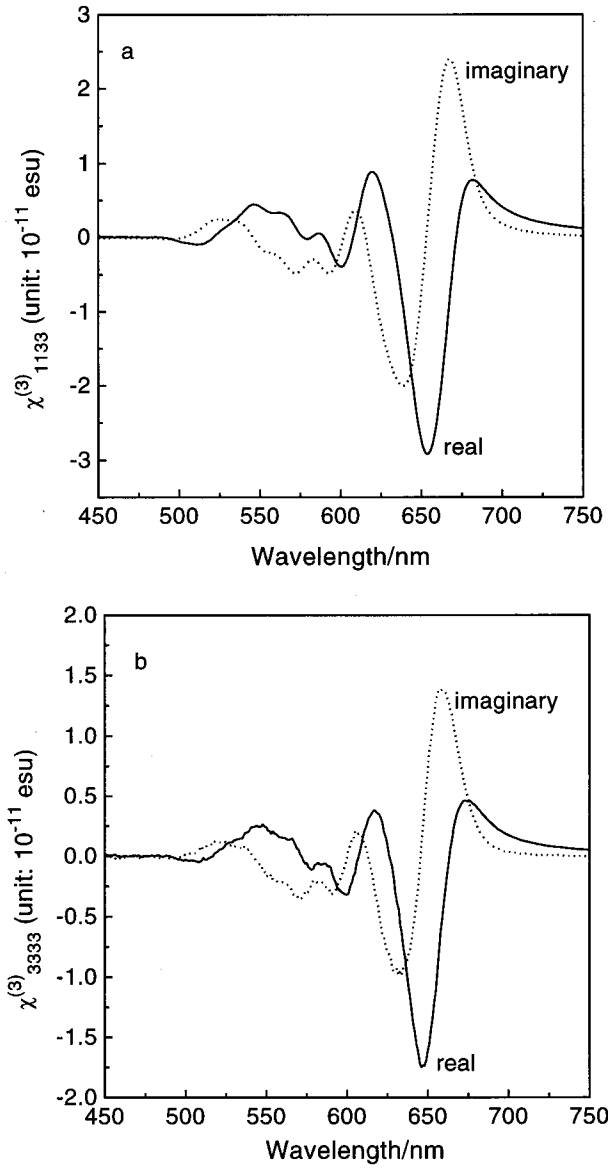

Figure 8. (a) Dispersion of $\chi^{(3)}_{1133}$ of 30 bilayers of the small poly-DCHD/PDAC film. Uncertainty: $\pm 1.4 \times 10^{-12}$ esu. (b) Dispersion of $\chi^{(3)}_{3333}$ of 30 bilayers of the small poly-DCHD/PDAC film. Uncertainty: $\pm 1.8 \times 10^{-12}$ esu.

the absorption peak at 650 nm are located near 671 and 646 nm, respectively, in Im[$\chi^{(3)}_{1133}$] and Im[$\chi^{(3)}_{3333}$].

Table 1 lists the peak values of the third-order NLO susceptibility of large poly-DCHD/PDAC films at the wavelength region of the main backbone absorption. These values are of the same order of magnitude when compared to the values of $\chi^{(3)}$ for polydiacetylenes with different side groups obtained by electroabsorption spectroscopy.[30] Similar electroabsorption spectra of the small poly-DCHD/PDAC multilayers are also measured, and the results are presented in Figure 8a ($\chi^{(3)}_{1133}$) and Figure 8b ($\chi^{(3)}_{3333}$). In comparison with Figure 7a and 7b, even though the shapes of the corresponding spectroscopic curves between the two samples are very similar, the obvious differences in peak positions and magnitudes can be seen from these spectra. The changes of electroabsorption peak positions are originated from the difference of absorption bands due to the different electron delocalization lengths in the large and small poly-DCHD nanocrystals. For the small poly-DCHD, the absorption shoulder near 595 nm corresponds to the electroabsorption peaks at 592 and 608 nm, and the absorption peak at 638 nm corresponds to the electroabsorption peaks at 635 and 663 nm. Table 2 summarizes the third-order NLO values of the small poly-DCHD films at several peak wavelengths. The

average ratio of $\chi^{(3)}_{3333}$ to $\chi^{(3)}_{1133}$ is 0.6, significantly smaller than that of the large poly-DCHD nanoparticles, indicating that the orientation of main backbone of the smaller poly-DCHD parallel to the plane of the substrate is further improved and predominantly in-plane orientation of the polydiacetylene backbone is obtained. Clearly, nanocrystals have adsorbed onto the substrate with the crystal facets containing the polymer backbones.

5. Conclusion

Two different sized polymeric nanocrystals, poly-DCHD, can be fabricated into composite films by the ESA technique using PDAC as the oppositely charged polyelectrolyte. UV−visible absorption and AFM images show that the composite films are uniform. The chromophore (polydiacetylene main backbone) orientation and third-order nonlinearity of poly-DCHD/PDAC multilayers were investigated by electroabsorption spectroscopy. The ratios of $\chi^{(3)}_{3333}$ to $\chi^{(3)}_{1133}$ are significantly less than 3 for both films, indicating that the polymer chains are predominantly parallel to the plane of the substrate. From the standpoint of planar fabrication, this is the desired preferred orientation where the in-plane component of the nonlinear optical coefficient $\chi^{(3)}_{1111}$ is expected to be the largest. The films showed appreciable third-order nonlinearity of the order of 10^{-11} esu for the tensorial components $\chi^{(3)}_{3333}$ and $\chi^{(3)}_{1133}$.

Acknowledgment. This work is partially supported by funding from the ONR.

References and Notes

(1) Ulman, A. *An Introduction to Ultrathin Films, From Langmuir−Blodgett to Self-Assembly*; Academic: Boston, 1991.
(2) Weller, H. *Angew. Chem., Int. Ed. Engl.* **1993**, *32*, 41.
(3) Colvin, V. L.; Schlamp, M. C.; Alivisatos, A. P. *Nature* **1994**, *370*, 354.
(4) Cassagneau, T.; Mallouk, T. E.; Fendler, J. H. *J. Am. Chem. Soc.* **1998**, *120*, 7848.
(5) Fendler, J. H. *Chem. Mater.* **1996**, *8*, 1616 and references therein.
(6) Weller, H. *Angew. Chem., Int. Ed. Engl.* **1996**, *35*, 1079.
(7) Jenekhe, S. A.; Chen, X. L. *Science* **1998**, *279*, 1903.
(8) Bloor, D.; Chance, R. R. *Polydiacetylenes, NATO ASI Series*; Martinus Nijhoff: Dordrecht, Boston, 1985.
(9) Sandman, D. J. *Trends Polym. Sci.* **1994**, *2*, 44.
(10) Sandman, D. J. *Polymeric Materials Encyclopedia*; Salamone, J. C., Ed.; CRC Press: Boca Raton, FL, 1996; vol. 2, p 1468.
(11) Ohnuma, H.; Hasegawa, K.; Se, K.; Kotaka, T. *Macromolecules* **1985**, *18*, 2339.
(12) (a) Yang, Y.; Lee, J. Y.; Jain, A. K.; Kumar, J.; Tripathy, S. K.; Matsuda, H.; Okada, S.; Nakanishi, H. *J. Phys.: Condens. Mater.* **1991**, *3*, 9563. (b) Yang, Y.; Lee, J. Y.; Li, L.; Kumar, J.; Jain, A. K.; Tripathy, S. K. *MRS Proceedings* **1992**, *247*, 729.
(13) (a) Kajzar, F.; Messier, J.; Ledoux, J. *Opt. Commun.* **1983**, *45*, 133. (b) Carter, G. M.; Chen, Y. J.; Tripathy, S. K. *Appl. Phys. Lett.* **1983**, *43*, 891.
(14) Herold, M.; Schmid, W.; Vogtmann, T.; Fischer, R.; Haarer, D.; Schwoerer, M. *Appl. Opt.* **1995**, *34*, 996.
(15) Sauteret, C.; Hermann, J.-P.; Frey, R.; Pradere, F.; Ducuing, J. *Phys. Rev. Lett.* **1976**, *36*, 956.
(16) Kasai, H.; Nalwa, H. S.; Oikawa, H.; Okada, S.; Matsuda, H.; Minami, N.; Kakuta, A.; Ono, K.; Mukoh, A.; Nakanishi, H. *Jpn. J. Appl. Phys.* **1992**, *31*, L1132.
(17) Yase, K.; Hanada, T.; Kasai, H.; Sato, T.; Okada, S.; Oikawa, H.; Nakanishi, H. *Mol. Cryst. Liq. Cryst.* **1996**, *294*, 71.
(18) Kasai, H.; Kamatani, S.; Okada, S.; Oikawa, H.; Matsuda, H.; Nakanishi, H. *Jpn. J. Appl. Phys.* **1996**, *34*, L211.
(19) Thakur, M.; Meyler, S. *Macromolecules* **1985**, *18*, 2341.
(20) Carter, G. M.; Chen, Y. J.; Tripathy, S. K. *Opt. Eng.* **1985**, *24*, 609.
(21) Mann, S.; Oldroyd, A. R.; Bloor, D.; Ando, D. J.; Wells, P. J. *SPIE Proceedings* **1988**, *971*, 245.
(22) Rochford, K. B.; Zanoni, R.; Gong, Q.; Torruellas, W. E.; Stegeman, G. I. *SPIE Proceedings* **1989**, *1147*, 279.
(23) Tripathy, S. K.; Katagi, H.; Kasai, H.; Balasubramanian, S.; Oshikiri, H.; Kumar, J.; Oikawa, H.; Okada, S.; Nakanishi, H. *Jpn. J. Appl. Phys.* **1998**, *37*, L343.
(24) Decher, G. *Science* **1997**, *277*, 1232.
(25) (a) Kotov, N. A.; Dekany, I.; Fendler, J. H. *J. Phys. Chem.* **1995**, *99*, 13065. (b) Ariga, K.; Lvov, Y.; Kunitake, T. *J. Am. Chem. Soc.* **1997**, *119*, 2224. (c) Lvov, Y.; Ariga, K.; Ichinose, I.; Kunitake, T. *J. Am. Chem. Soc.* **1995**, *117*, 6117. (d) Onda, M.; Lvov, Y.; Ariga, K.; Kunitake, T. *Biotech. Bioeng.* **1996**, *51*, 163. (e) Lvov, Y.; Decher, G.; Sukhorukov, G. *Macromolecules* **1993**, *26*, 5396. (f) Cheung, J. H.; Stockton, W. B.; Rubner, M. F. *Macromolecules* **1997**, *30*, 2712.
(26) (a) Balasubramanian, S.; Wang, X. G.; Wang, H. C.; Yang, K.; Kumar, J.; Tripathy, S. K. *Chem. Mater.* **1998**, *10*, 1554. (b) Wang, X. G.; Balasubramanian, S.; Li, L.; Jiang, X. L.; Sandman, D. J.; Rubner, M. F.; Kumar, J.; Tripathy, S. K. *Macromol. Rapid Commun.* **1997**, *18*, 451.
(27) (a) He, J.-A.; Samuelson, L.; Li, L.; Kumar, J.; Tripathy, S. K. *Langmuir* **1998**, *14*, 1674. (b) He, J.-A.; Samuelson, L.; Li, L.; Kumar, J.; Tripathy, S. K. *J. Phys. Chem. B* **1998**, *102*, 7067.
(28) Katagi, H.; Kasai, H.; Okada, S.; Oikawa, H.; Matsuda, H.; Liu, Z.-F.; Nakanishi, H. *Jpn. J. Appl. Phys.* **1996**, *35*, L1364.
(29) Katagi, H.; Kasai, H.; Okada, S.; Oikawa, H.; Matsuda, H.; Nakanishi, H. *J. M. S.- Pure Appl. Chem.* **1997**, *A34*, 2013.
(30) Yang, K.; Kim, W.; Kumar, J.; Li, L.; Tripathy, S. K. *Opt. Commun.* **1997**, *144*, 252.
(31) Yang, K.; Cheong, D.-W.; Tripathy, S. K.; Kumar, J. *Opt. Commun.* **1997**, *144*, 259.
(32) Yang, K.; Wang, X. G.; Kumar, J.; Jain, A.; Li, L.; Tripathy, S. K. *Nonlinear Optics* **1998**, *19*, 215.
(33) Yang, K.; Balasubramanian, S.; Wang, X. G.; Kumar, J.; Tripathy, S. K. *Appl. Phys. Lett.* **1998**, *73*, 3345.
(34) Rohl, P.; Andress, B.; Nordmann, J. *Appl. Phys. Lett.* **1991**, *59*, 2793.
(35) (a) Stockton, W. B.; Rubner, M. F. *Macromolecules* **1997**, *30*, 2717. (b) Wang, L. Y.; Fu, Y.; Wang, Z. Q.; Fan, Y. G.; Zhang, X. *Langmuir* **1999**, *15*, 1360.
(36) (a) Fritz, M.; Radmacher, M.; Cleveland, J. P.; Allersma, M. W.; Stewart, R. J.; Gieselmann, R.; Janmey, P.; Schmidt, F. C.; Hansma, P. K. *Langmuir* **1995**, *11*, 3529. (b) Caruso, F.; Furlong, D. N.; Ariga, K.; Ichinose, I.; Kunitake, T. *Langmuir* **1998**, *14*, 4559.
(37) Kawabe, Y.; Jarka, F.; Peygambarian, N.; Guo, D.; Mazumdar, S.; Dixit, S. N.; Kajzar, F. *Phys. Rev. B* **1991**, *44*, 6530.
(38) Heldmann, C.; Brombacher, L.; Neher, D.; Graf, M. *Thin Solid Films* **1995**, *261*, 241.